Analysis of peel arm curvature for the determination of fracture toughness in metal-polymer laminates

L. F. KAWASHITA, D. R. MOORE*, J. G. WILLIAMS
Mechanical Engineering Department,Imperial College London, London, SW7 2AZ, UK
E-mail: r.moore@imperial.ac.uk

Variable angle fixed arm peel and mandrel peel tests were performed on four metal-polymer laminate systems. In total, four polymeric adhesives and three grades of aluminium alloy (AA) substrates were used, enabling a wide range of material properties to be encompassed in the study. Mandrel peel tests provided a direct determination of the plastic bending energy (G_p) and adhesive fracture toughness (G_a). For the fixed arm tests, a global energy-balance analysis (*ICPeel* software) was used to determine G_a and G_p analytically. This was done via the calculation of the maximum curvature of the peel arm ($1/R_0$) and the root rotation angle (θ_0) from a beam on elastic foundation model. In order to investigate the accuracy of the analytical approach, an experimental method based on high resolution digital photography enabled $1/R_0$ and θ_0 to be measured independently. It was then possible to compare these parameters by measurement and by analytical approach (ICPeel software). θ_0 and R_0 relate to the slope and curvature of the peel arm at the debonding front, respectively. In order to measure these parameters, the coordinates of the edge of the peel arm were extracted from each digital photograph, and the slope and curvature were calculated numerically from these curves. The crack tip was then defined as the point of maximum curvature $1/R_0$, in accordance with traditional beam theory. It was found that the smoothing in the calculation of first and second derivatives could generate significant errors in the value of θ_0. On the other hand, R_0 was found to be a more robust measurement, with little dependence on smoothing. Nevertheless, on most occasions, the measured values of θ_0 and R_0, as well as the resulting G_a were shown to be in good agreement with the analytical model. Since the peel fractures were generally cohesive, G_a was compared with the cohesive fracture toughness (G_c) obtained from Tapered Double Cantilever Beam (TDCB) tests with a fracture mechanics analysis. Good agreement was observed, confirming that G_a is likely to be a geometry-independent fracture parameter.
© *2005 Springer Science + Business Media, Inc.*

1. Introduction

Adhesively bonded joints are widely used in aerospace, automotive and electronics applications, where knowledge of the quality of the bonding is of significant technological value. This is often measured by peel strength—the force per unit width required to peel the laminate apart. This however does not separate adhesive fracture toughness (G_a) from plastic work in bending (G_p), which can be up to 90% of the total input energy (G). An analytical energy-balance approach [1–3] has been used to estimate the adhesive fracture toughness from fixed-arm and T-peel tests. The mechanical properties of the substrates are given either as bilinear or power-law work hardening stress-strain curves. By assuming a beam on an elastic foundation model, the rotation at the root (θ_0) and the maximum curvature of the substrate ($1/R_0$) are estimated. Large displacement beam theory is used in the calculation of G_p, which is then subtracted from the total external work G to give G_a.

Full details of the energy-balance model are given elsewhere [1, 2] and only simplified expressions will be used here. Neglecting any tensile deformation of the peel arm, which is usually small, the adhesive fracture energy is given by:

$$G_a = G - G_p \tag{1}$$

The plastic work in bending is calculated via the integration of the moments acting on the peel arm during the bending/unbending process. Analytical expressions of G_p have been derived, and the only unknown is the

*Author to whom all correspondence should be addressed.
0022-2461 © *2005 Springer Science + Business Media, Inc.*
DOI: 10.1007/s10853-005-0856-8

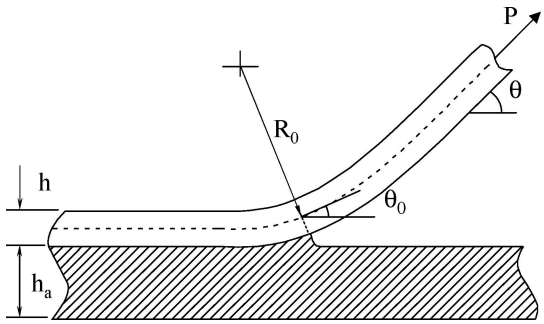

P	Peel force [N]
θ	Peel angle [rad]
h	Peel arm thickness [mm]
h_a	Bond line thickness [mm]
R_0	Radius of curvature at the root [mm]
θ_0	Root rotation [rad]

Figure 1 Fixed arm peel parameters.

maximum curvature $1/R_0$ to which the peel arm is subjected (Fig. 1).

Introducing a normalised curvature given by:

$$k_0 = \frac{h}{2\varepsilon_y}\frac{1}{R_0} \tag{2}$$

the plastic bending energy is then given by:

$$G_p = \frac{E\varepsilon_y^2 h}{2} f(k_0) \tag{3}$$

where ε_y is the yield strain of the peel arm and $f(k_0)$ is the area inside the normalised moment-curvature diagram [2]. $f(k_0)$ is dependent on the material model and work hardening coefficient. For a bilinear model (as used in this work), expressions for $f(k_0)$ are given in Appendix 1. If the adhesive layer under the attached peel arm is assumed to have linear-elastic stiffness, the relation between root rotation θ_0 and maximum curvature k_0 is given by:

$$\theta_0 = (2\varepsilon_y k_0)\sqrt{0.2 + \sqrt{0.058 + \frac{h_a E}{3hE_a}}} \tag{4}$$

where E is the elastic modulus of the peel arm, E_a is the elastic modulus of the adhesive layer, h is the thickness of the peel arm and h_a is the thickness of the adhesive layer.

The tensile stress-strain ($\sigma - \varepsilon$) curve of a metallic peel arm is fitted to either a bilinear or a power law work hardening function [2] in order to enable the use of analytical solutions. Although both models can be successful, the aluminium alloys often showed a better fit to a bilinear function and therefore only this model is used in this work. It is of the form:

$$\sigma = E\varepsilon \quad \text{for } \varepsilon \le \varepsilon_y,$$

and

$$\sigma = E\varepsilon_y + \alpha E\left(\varepsilon - \varepsilon_y\right) \quad \text{for } \varepsilon > \varepsilon_y \tag{5}$$

α is the work hardening coefficient, i.e. the ratio of plastic modulus to elastic modulus.

A direct experimental approach using a mandrel peel test can also be used for the determination of G_a [4, 5]. This involves deforming the peel arm around a roller and applying an alignment force to assure good conformation. The use of this method for metal-polymer laminates has shown promise [4–6].

This direct experimental approach has the advantage of not relying on any analytical theory, and it does not require a mechanical model for the peel arm material. However, there may be occasions when the particular geometry of a T-peel or fixed arm peel methods would be preferred. Consequently, reliance on a theoretical analysis of such procedures needs to be accommodated.

By measuring the geometrical parameters involved in the analytical procedure, then the accuracy of these methods could be routinely audited. The present work proposes the optical measurement of maximum curvature of the peel arm ($1/R_0$) and root rotation angle (θ_0) via high-resolution digital photography. Therefore, the adhesive fracture toughness G_a could be determined for each laminate by four different methods:

1. Fixed-arm peel with *ICPeel* analysis.
2. Fixed-arm peel with measured R_0.

TABLE I Materials and geometries

Sample	Adhesive	Substrates	Peel arm thickness (mm)	Bond line thickness (mm)	Dimensions of peel arm (bond line) (mm)
ESP 110/5754-0	ESP110 (rubber-toughened epoxy paste adhesive, general purpose)	AA 5754-O	1.00	0.40	15×200 (15×180)
Adhesive F/2024-T3	Adhesive-F (toughened epoxy film adhesive, cured in an autoclave)	AA 2024-T3	0.63	0.12	15×350 (15×300)
PP/5154-0	Polypropylene (bonded in a continuous industrial process)	AA 5154-O	0.24	0.95	20×200 (20×180)
XD4600/5754-0	XD4600 (rubber-toughened epoxy paste adhesive, automotive applications	AA 5754-0	1.00	0.25	15×200 (15×180)

3. Fixed-arm peel with measured θ_0.
4. Mandrel peel test.

The purpose of this paper is to investigate if these approaches have practical merit for metal-polymer laminates and to comment on the consequences.

2. Materials and specimen preparation

Four different types of laminates were used in the experimental work, and Table I summarises the characteristics of each sample. The adhesives were *ESP110* (a rubber toughened epoxy adhesive for general engineering applications), *Adhesive-F* (a toughened epoxy system for aerospace applications), a *polypropylene* (PP) polymer and *XD4600* (a rubber toughened epoxy adhesive for automotive applications). The substrates were aluminium alloys (AA) 5754-O, 5154-O and 2024-T3.

For ESP110/5754-O laminates, the substrates were blasted with alumina grit (mesh 400) and etched in a chromic acid solution for 30 min at 60°C. Cure took place in a hot air oven for 45 min at 150°C. Adhesive-F/2024-T3 laminates were initially prepared as panels and later machined into individual specimens. The surfaces were treated in a FPL-type etching process and primed with an aerospace-grade epoxy compound. The laminates were cured in an autoclave for 1 h at 132°C at a pressure of 2.8 bar. The PP/5154-O laminate consisted of two thin aluminium foils bonded by a polypropylene layer (for the fixed-arm tests, one of the sides was bonded to a rigid base plate). For XD4600/5754-O laminates, the substrates were also grit blasted and chromic acid etched. The laminates were cured at 150°C for 15 min followed by another 15 min at 190°C.

In all cases the sides of the specimens were carefully polished in order to produce sharp, plane edges, necessary for greater accuracy in the photographic technique.

3. Experimental procedure

Fixed-arm [7] and mandrel peel experiments [4] were conducted on an Instron universal testing machine. In all cases the crosshead speed was adjusted in order to give a constant 5 mm/min crack growth, and tests were performed at standard air conditions (21°C, 55% RH). Data were collected over lengths of at least 50 mm, and at least five specimens were tested per sample.

Fixed-arm tests were performed at 45°, 90° and 135° angles. The measurement of substrate curvature involved high quality digital photography and a subsequent image analysis that determined the local radius of curvature. The photography also provided means of measuring the root rotation.

The mandrel peel procedure is presented in detail elsewhere [4, 6]. The peel arm is bent around a circular roller whilst an alignment force is applied to the base of the laminate. From an unbonded laminate the plastic work in bending and coefficient of friction are obtained, and from a bonded laminate the adhesive fracture toughness is measured. Mandrel radii were available in the range 5 mm to 20 mm, and alignment forces up to 50 N/mm were used.

Tensile stress-strain measurements were conducted on all peel arm materials at 1 mm/min (strain rate 2×10^{-4} s^{-1}) where an optical extensometer was used to measure axial strain.

TABLE II Tensile stress-strain data for peel arm materials (bilinear fit up to 5% strain)

Peel arm material	E (GPa)	σ_y (MPa)	ε_y (%)	α
AA 2024 T3	70	360	0.510	0.035
AA 5754-O	69	108	0.160	0.027
AA 5154-O	74	145	0.195	0.010

4. Results and discussion

4.1. Uniaxial tensile tests

The best fit to the experimental tensile stress-strain data was found by limiting the curves to a maximum strain of 5%, which is above the deformation encountered by a peel arm in any of the peel tests. Table II summarises the tensile stress-strain results for the peel arms with a bilinear fit. The small values for yield strain reinforces the importance in using extensometers for gathering pre-yield data for the determination of elastic modulus.

4.2. Root curvature and rotation

A high-resolution digital camera fitted with macro lenses produced photographs of the specimens during the peeling process, and a personal computer recorded the photographs automatically. Computer programs were developed for an automatic computation of local curvatures. Fig. 2 illustrates the methodology for this calculation.

In order to make the calculations less sensitive to translations or rotations of the images, the x-y coordinates are parameterised by the arc length s over the upper edge of the peel arm. The origin of s is unimportant, and was arbitrarily taken as the left-most pixel in

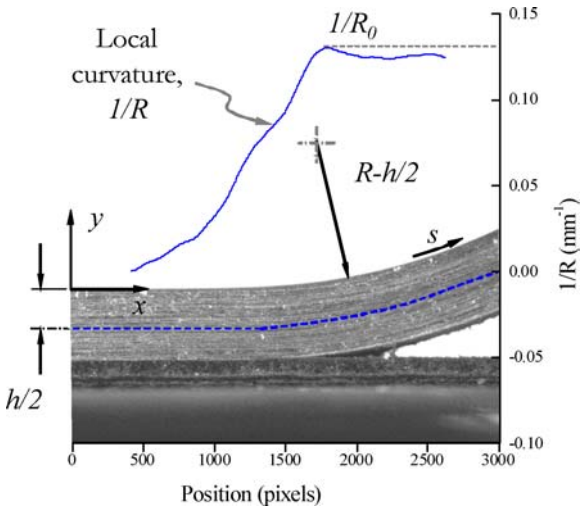

Figure 2 An illustration of curvature measurement using digital photography. The radius of curvature of the neutral line (R) is the radius of the upper edge plus half of the peel arm thickness ($h/2$).

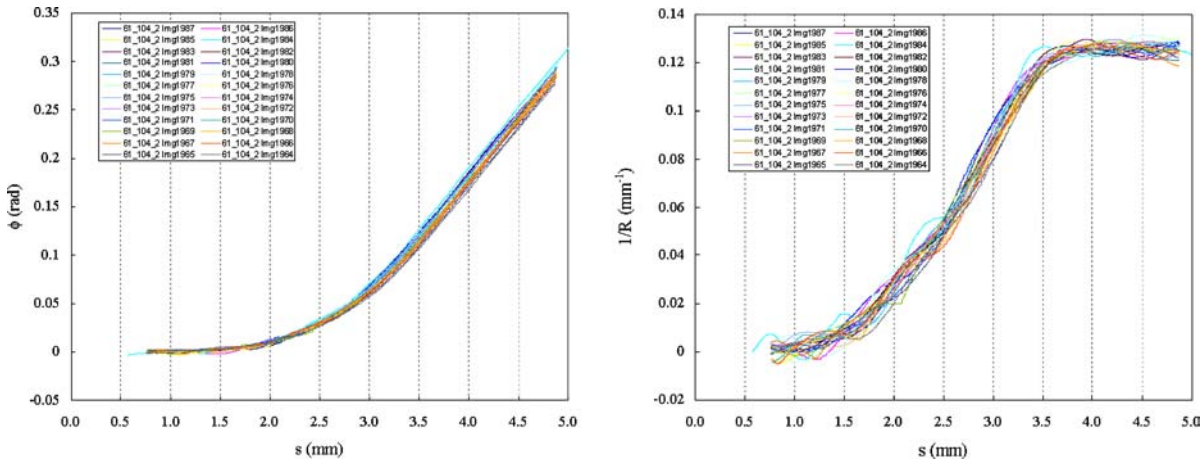

Figure 3 Slope (ϕ) and curvature ($1/R$) plotted against arc length s. Data relate to ESP110/5754-O.

the image. With reference to Fig. 2, the slope ϕ of the peel arm can be expressed as:

$$\phi = \frac{dy}{dx} = \frac{dy}{ds}\frac{ds}{dx} = \frac{y'}{x'} \tag{6}$$

where $x(s)$ and $y(s)$ are the parameterised coordinates and $\prime = \frac{d}{ds}$. The local curvature is given by

$$\frac{1}{R - (h/2)} = \frac{x''y' - x'y''}{\left[(x')^2 + (y')^2\right]^{3/2}}. \tag{7}$$

where $'' = \frac{d^2}{ds^2}$ and $h/2$ is half of the peel arm thickness (since R is the radius of the neutral axis of the peel arm). The root rotation θ_0 is therefore the value of ϕ at the crack tip, and the root curvature R_0 is the value of R at the crack tip. Making s_o the point on the upper edge nearest to the crack tip, then $\theta_0 = \phi(s_o)$ and $R_0 = R(s_o)$.

The calculations of first and second derivatives of $x(s)$ and $y(s)$ require a smoothing procedure since these are a series of discrete points (pixels) instead of continuous functions [8, 9]. This is detailed in Appendix 2. In turn, ϕ and $1/R$ can be plotted against the arc length s, as illustrated in Fig. 3. It can be seen from Equations 6 and 7 that ϕ is defined in terms of first derivatives and $R(s)$ in terms of first *and* second derivatives. Therefore, the individual values of R would be expected to carry larger errors than those due to ϕ. This is also illustrated in Fig. 3 where there is greater scatter in the data for $1/R$.

θ_0 and R_0 are those values of φ and R at the crack tip; therefore the value of s_o for the crack tip has to be accurately defined. The digital photography includes the crack tip but this could not be used directly for defining these co-ordinates. Although the edge of the peel arm could be easily extracted from each image, the crack tip showed extensive micro-cracking and stress-whitening phenomena, which prevented a clear definition of its location. Therefore, the peak in local curvature was used as a definition of 'effective' crack tip, i.e. $1/R(s_o) = \max(1/R_{(s)})$. Two issues arise from this approach. First, the adopted definition of crack tip also relies on second derivatives. Second, ϕ changes significantly with a change in s. It transpires that θ_0 is strongly dependent on the *position* of the peak in curvature, while R_0 is basically the *value* of this peak.

Consequently, it was found that the value of θ_0 is very sensitive to the smoothing procedure, while R_0 is very insensitive to this process. This is because the location of s_o varies as the curves become smoother, but the value of maximum curvature changes little.

The radius of curvature at the root R_0 could be calculated theoretically via a beam on elastic foundation model (*ICPeel* software) [10]. A comparison of measured radius of curvature with calculated radius of curvature shows excellent agreement, particularly when there is a good fit of stress-strain data to a bilinear function (as in the case of the aluminium alloys used in this study). This is shown in Fig. 4 for and Fig. 5 for two of the laminates.

There are three ways of obtaining a value of root rotation angle, namely by direct measurement (for which there are two options), by calculation from *ICPeel* [10] and by calculation from a measured value of R_0 (Equation 4). The two methods of measurement of θ_0 differ in the way the crack tip is located, either *numerically* by the peak in local curvature (as previously discussed) or *visually* via the direct observation of the photographs.

The direct measurement of angle θ_0 is achieved by locating the crack tip from the photographs and

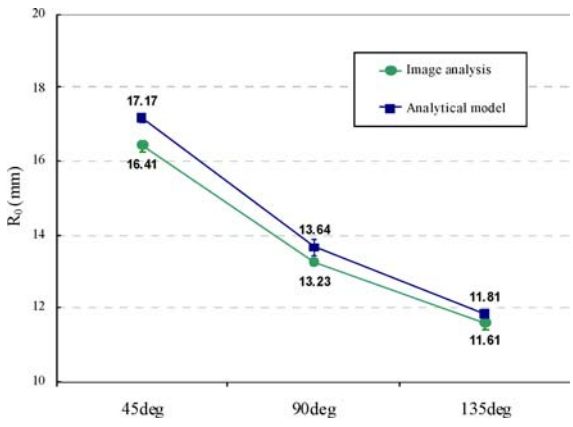

Figure 4 Calculated versus measured R_0 for ESP110/ 5754-0 (offset zero).

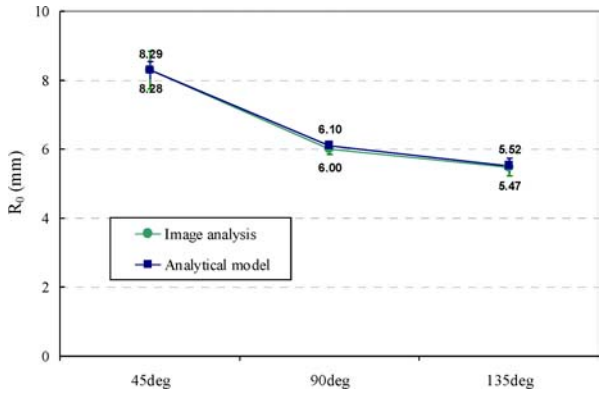

Figure 5 Calculated versus measured R_0 for Adhesive F/ 2024 T3.

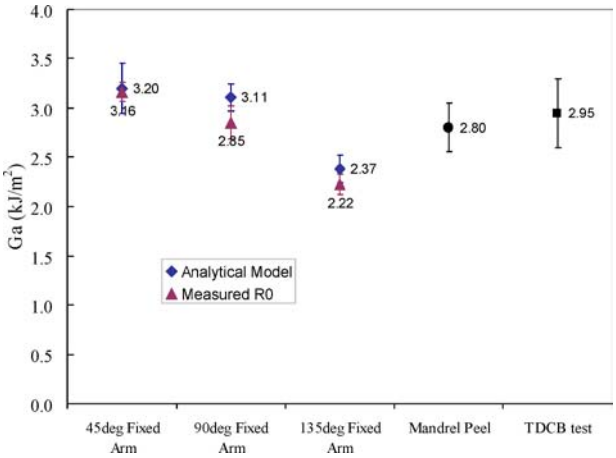

Figure 7 Adhesive fracture toughness results for Adhesive-F / 2024-T3.

measuring the slope of the peel arm at this point. However, there can be some practical problems with this approach. First, the angle might be small and in general, the smaller the angle the larger the percentage error of measurement. Second, micro-cracking and deformations in the adhesive layer may 'blur' the definition of the crack tip. However, previous attempts with this method for measuring the root rotation angle [1] for polymeric laminates did record some success. For that study, the measured values of θ_0 were relatively large (e.g. 20 to 60°). Nevertheless, the authors recorded errors of measurement for θ_0 of ±6°, which is acceptable for those relatively large angles, and there was reasonable agreement between calculated and measured values for θ_0. Unfortunately, with metal-polymer laminates both problems were prevalent and therefore the direct measurement of θ_0 was not found to have sufficient accuracy.

Meanwhile, the measurement of θ_0 via the peak in local curvature showed sensitivity to the smoothing procedures (see Appendix 2), producing large percentile errors in the value of θ_0 since the angles were small.

The current inconsistency in determining a measurement of θ_0 has prevented our use of this approach for the determination of G_a. However, it is anticipated that in future a method should be possible.

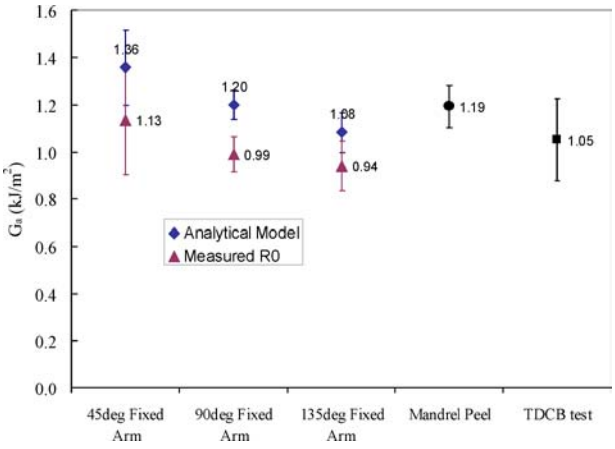

Figure 6 Adhesive fracture toughness results for ESP110 / 5457-O.

4.3. Adhesive fracture toughness (G_a)

For the fixed arm peel experiments (in all three peel angles), G_a was calculated from only two approaches after the root rotation methodology was eliminated:

(i) Calculation of plastic work in bending based on the measured peel arm curvature (R_0 *Measurement*);
(ii) Full analytical solution (*ICPeel*).

G_a was also measured directly by the mandrel peel test. In addition the cohesive fracture toughness of the adhesive was measured using Tapered Double Cantilever Beam (TDCB) geometry, according to an European Society for Structural Integrity (ESIS) test protocol [7].

Fig. 6 shows the results for adhesive fracture toughness for the ESP110/5457-O laminates. The determinations of G_a based on measured R_0 and calculated R_0 show agreement within the scatter bands of measurement. There is also agreement with the G_a value from the mandrel test. All failures are cohesive, although there is far less adhesive coating on the peel arm than that left on the base plate. However, agreement with the cohesive fracture toughness from the TDCB test is good. Therefore, in general it would be reasonable to suggest that all data were in agreement to within experimental error, as defined by the measurement scatter bands.

Fig. 7 shows the results for Adhesive-F/2024-T3. Cohesive fractures were observed at the lower fixed-arm peel angles and in the mandrel tests with low alignment forces. These adhesive fracture toughness values show agreement and also agree with the cohesive fracture toughness from the TDCB test.

Some interfacial failure was observed in the fixed arm peel tests as the peel angle increased. In general there is reasonable agreement between G_a derived by the analytical model and measured R_0. The peel test at a fixed peel angle of 135° exhibited the highest level of adhesive fracture and not surprisingly a lower value was obtained for the fracture toughness. Yet, good agreement occurred between the G_a values based on calculated and measured R_0.

Fig. 8 shows results for XD4600/5754-0 laminates where again there is generally good agreement between

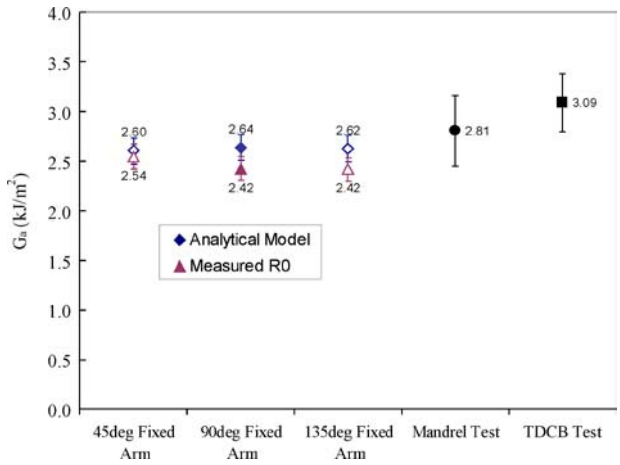

Figure 8 Adhesive fracture toughness results for XD4600 / 5457-O.

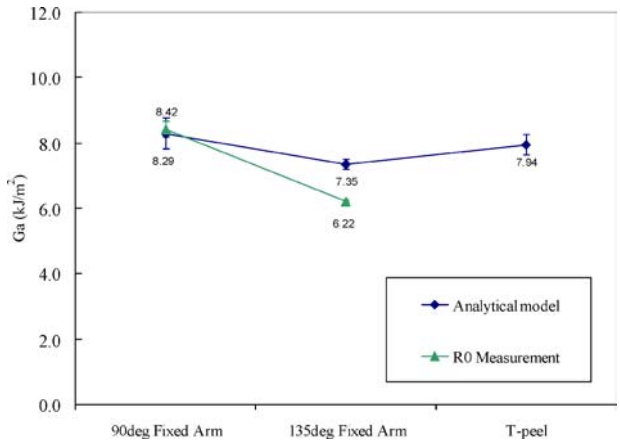

Figure 9 Adhesive fracture toughness results for PP/5154-O.

each of the methods. The G_a values from the fixed arm tests agree well between determinations based on *ICPeel* and *measured* R_0. All peel fractures were cohesive, although only a small coating of adhesive was observed on the peel arm. Nevertheless, the cohesive fracture toughness showed agreement with the G_a values by both fixed arm and mandrel peel, although only just within the scatter bands of measurement.

The results for the PP/5154-O laminate are shown in Fig. 9 where it can be seen that a less extensive set of measurements were made. In particular, there are no mandrel or TDCB measurements.

It was not possible to conduct measurements at small angles in the fixed arm test, since the peel forces were sufficiently large that the peel arm fractured. Nevertheless, the agreement between the values of G_a by R_0 measurement and R_0 calculation through *ICPeel* software is reasonable. However, the limited database for this laminate could not include scatter bands for the G_a by R_0 measurement.

5. Concluding comments

Results on four different aluminium laminate systems have enabled the measurement of root rotation and radius of curvature of the peel arm to be made. High-resolution digital photography is involved in both measurements. The root rotation angle can be determined from the first derivative of the co-ordinates of the peel arm curvature. The value of θ_0 must relate to the crack tip. In turn, the co-ordinates of the crack tip can be obtained at the maximum curvature of the peel arm. Unfortunately, this is only possible when the resolution of the digital photography is high and the smoothing of the curvature data below a certain level. In time, such conditions will be routinely achievable, but this was not always so in the experimental results reported here. Nevertheless, the principles of measurement have been established.

Measurement of radius of curvature for the peel arm can however be made with good accuracy, and these data are not sensitive to the smoothing of the local curvature data. It certainly agrees well with calculated values of radius of curvature using *ICPeel* software. Moreover, when the measured value of R_0 is used to determine plastic bending energy and in turn adhesive fracture toughness, the G_a values agree well with those from direct experimental determination of adhesive fracture toughness, as obtained in a mandrel peel procedure.

The stress-strain behaviour of the aluminium alloy substrates used in this study could be described accurately by a bilinear function. Therefore, the analytical method used for calculating R_0 would be expected to be reasonable. However, the advent of being able to measure this curvature means that on any other occasion when the fit of the stress-strain data might not be so good, that a combination of measured radius, peel strength and deformational behaviour for the peel arm can still lead to an accurate value for plastic bending energy and in turn adhesive fracture toughness. Therefore, this combination of measurements can accommodate test geometries such as fixed arm peel and T-peel for an objective determination of adhesive fracture toughness.

A mandrel peel procedure remains a viable direct method for measuring adhesive fracture toughness.

Both fixed arm and mandrel peel methods gave cohesive peel fractures. However, the thickness of adhesive on the peel arm was often quite small. Nevertheless, the G_a values showed good agreement with cohesive fracture toughness values obtained from TDCB fracture tests. This suggests that adhesive fracture toughness obtained form a peel test is providing a geometry independent value for peel toughness.

Acknowledgements

The authors acknowledge support from a Royal Academy of Engineering senior research fellowship for D R Moore and support from IMRE, Singapore for L. F. Kawashita

Appendix 1: $f(k_0)$ for a bilinear stress-strain model

There are three cases to consider in the determination of the $f(k_0)$ functions:

Case 1: Elastic bending and unbending

$$0 < k_0 \leq 1$$

then

$$f(k_0) = 0$$

Case 2: Plastic bending and elastic unbending

$$1 < k_0 \leq 2\frac{(1-\alpha)}{(1-2\alpha)}$$

then

$$f(k_0) = (1-\alpha)\left[\frac{1}{3}k_0^2 + \frac{2}{3k_0} - 1\right]$$

Case 3: Plastic bending and unbending

$$k_0 > 2\frac{(1-\alpha)}{(1-2\alpha)}$$

then

$$\begin{aligned} f(k_0) &= \frac{4}{3}\alpha\left[(1-\alpha)\left(1-\frac{\alpha}{2}\right) - \frac{1}{8}\right]k_0^2 + 2(1-\alpha) \\ &\times\left(1-\frac{\alpha}{2}\right)(1-2\alpha)k_0 + \frac{2(1-\alpha)}{3(1-2\alpha)k_0} \\ &\times\beta - (1-\alpha)\gamma \end{aligned}$$

where

$$\beta = \left[1 - 2\alpha^2(2-\alpha) + 4(1-\alpha)^3\right]$$

and

$$\gamma = \left[1 + 2\alpha(1-\alpha) + 4(1-\alpha)^2\right]$$

In practice, Case 3 is the most common.

Appendix 2: Smoothing procedures in the derivation of θ_0 and R_0

Fig. 2 (in the main text) illustrates a photograph of the curvature in the peel arm during peeling. The edge of the peel arm has to be defined in terms of the coordinates (x, y). These coordinates are then parameterised by the arc length s in order to give insensitivity to any rotation of the images. The first and second derivatives of the functions $x(s)$ and $y(s)$ then have to be obtained in order to use Equations 6 and 7 to calculate $\phi$and R, from which θ_0 and R_0 can then be derived.

The first ($' = \frac{d}{ds}$) and second ($'' = \frac{d^2}{ds^2}$) derivatives were computed by conducting a least-squares fit for each point along the curves of parameterised coordinates. Fig. A1 illustrates the calculation of the first derivative dx/ds (second derivatives were computed by applying the same procedure to the curves of first derivatives).

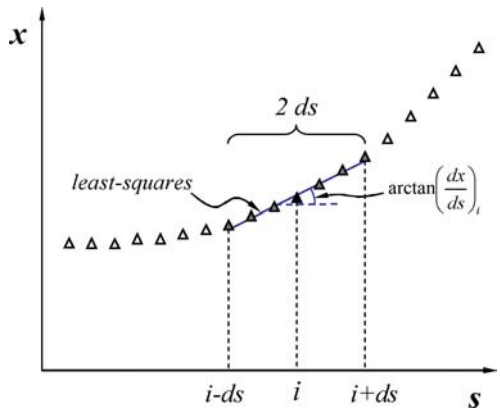

Figure A1 Calculation of derivatives with a convolving least-squares interval.

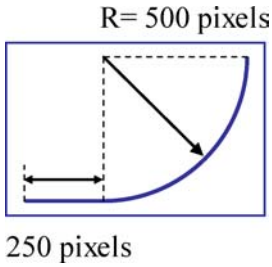

Figure A2 Dimensions of a simulation image.

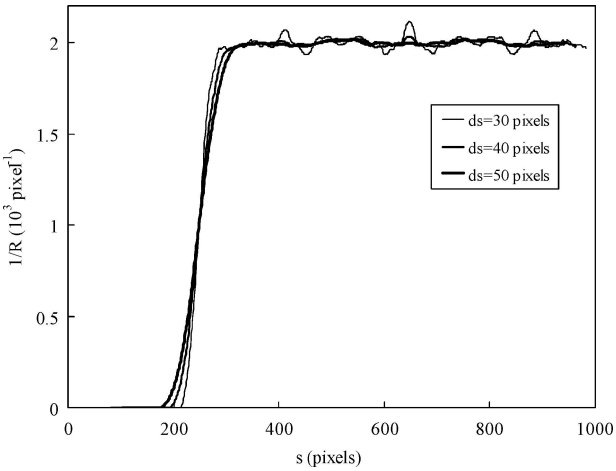

Figure A3 Local curvatures with different size intervals (ds).

The values of first and second derivatives are therefore dependent on the size of the interval from which the least-squares fits are calculated. This is defined by the distance $2ds$ (in pixels) where i is a central point (Fig. A1). Increasing ds will result in reduced noise, but if ds is excessively large then important features of the curves may be smoothed out. Therefore, an appropriate degree of smoothing should be found through optimising the value of ds.

In order to study the influence of the interval ds, a series of simulation images were analysed. These images consisted of a straight segment followed by an arc of 90° of constant radius, as shown in Fig. A2. Although several images with different radii were analysed, only the 500 pixel radius will be discussed here.

In this image the values of R_0 and θ_0 are 500 pixels and 0°, respectively. The methods for computing R_0

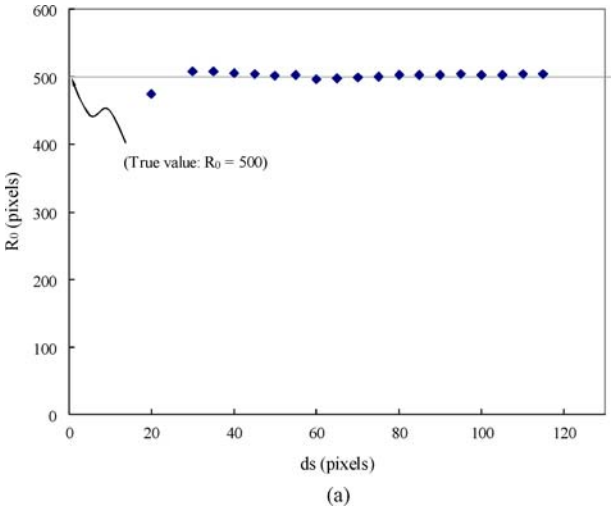

Figure A4a Radius of curvature R_0 as a function of smoothing interval *ds*.

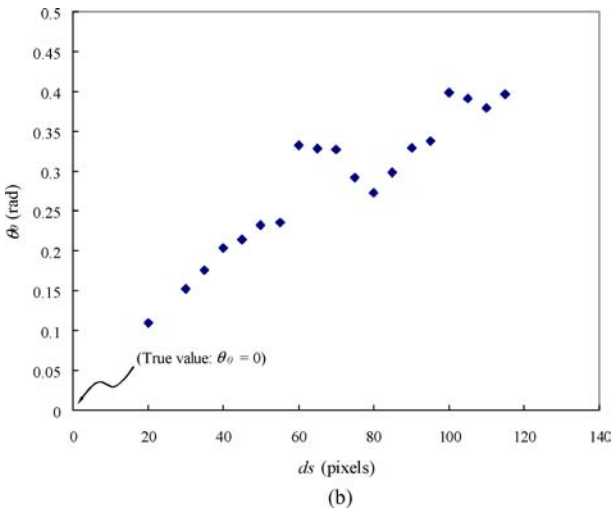

Figure A4b Root rotation θ_0 as a function of smoothing interval *ds*.

and θ_0 were then applied using different values of *ds*, and the effect of smoothing could be investigated.

Fig. A3 shows the local curvature calculated with three different values for *ds*. The smallest value of *ds* (30 pixels) produces the least smoothing and as a consequence some noise appears in the region of constant curvature, but the transition between zero curvature and the plateau is sharper and better defined. As *ds* is increased, the curve becomes smoother, but so does the transition region, and the edge of the plateau is shifted to the right.

Plots of $1/R$ versus s are used to define the onset of maximum curvature. θ_0 is then determined as the value of ϕ at this value of s. Consequently, as smoothing increases (larger values for *ds*), the edge of the plateau is shifted and this affects the value of θ_0 in quite a significant way. Fig. A4 shows the computed values of R_0 for the simulated image. Beyond a certain minimum *ds*, R_0 is very close to the true value and changes little with increasing smoothing.

The main difference between simulated and actual images is that in the latter the radius of curvature is not constant, but decreases gently from the crack tip onwards. This implies that, in actual images, a high degree of smoothing will also generate errors in the value of R_0. Therefore, an optimum value for *ds* should be large enough to avoid excessive noise, but small enough so that the peak in local curvature is not shifted excessively.

Unfortunately, there is no single optimum value for *ds*, but a simple criterion can be adopted. It was decided that the error in local curvature of a circular arc (going from 0 to 90°) should be below 5%. For the case in Fig. A3, a value of *ds* should be chosen so that the variations on the plateau are less than 5% of the average value. By analysing a series of computer-generated images, it was found that this criterion was satisfied when the length of *ds* covered approx. 4° of an arc.

However, in order to adopt this criterion, an estimative of the maximum curvature (in pixel^{-1}) should be available *before* the final measurement of local curvature. This was possible by the use of an iterative computer program that performed several calculations of local curvature with variable *ds* until the requirement was satisfied (however, it should be noticed that the value of R_0 does not vary significantly with a change in *ds*).

On the other hand, the value of θ_0 is strongly dependent on *ds*, as shown in Fig. A4. The true value for the simulation image, $\theta_0 = 0$, is actually never achieved. It seems that an extrapolation of these data to $ds = 0$ would give a good estimate of the true θ_0. However, below a certain value of *ds* the curves become dominated by noise and it is sometimes difficult to determine precisely when this occurs. The method has promise, but given its complexity the measurement of R_0 was preferred.

References

1. A. J. KINLOCH, C. C. LAU and J. G. WILLIAMS, *Int. J. Fract.* **66** (1994) 45 .
2. I. GEORGIOU, H. HADAVINA, A. IVANKOVIC, A. J. KINLOCH, V. TROPSA and J. G. WILLIAMS, *The Journal of Adhesion* **79** (2003) 239.
3. J. G. WILLIAMS, *J. Adhesion* **41** (1993) 225.
4. L. F. KAWASHITA, D. R. MOORE and J. G. WILLIAMS, *The Journal of Adhesion* **80** (2004) 147.
5. E. BRESLAUER and I. T. TROCYNSK, *J. Adhesion Sci. Technol.* **12**(4) (1998) 367.
6. L. F. KAWASHITA, D. R. MOORE and J. G. WILLIAMS, t.b.p. in *The Journal of Adhesion*, (2005).
7. D. R. MOORE, A. PAVAN and J. G. WILLIAMS, eds "Fracture Mechanics Testing Methods for Polymers, Adhesives and Composites", edited by D. R. Moore, and J. G. Williams, ISBN 008 0436897, p. 203 (Elsevier, Oxford, 2001), Ch. 3.
8. M. WORRING and A. W. M. SMEULDERS, *Image Understanding* **58**(3), (1993) p. 366.
9. V. KOVALEVSKY, *Int. J. Patt. Recog.* **15**(7), (2001).
10. *ICPeel Spreadsheet*, Imperial College London Website, www.me.ic.ac.uk/AACgroup

Received 3 February
and accepted 7 March 2005